Enhancement of cloud cover and suppression of nocturnal drizzle in stratocumulus polluted by haze

A. S. Ackerman,[1] O. B. Toon,[2] D. E. Stevens,[3] and J. A. Coakley Jr.[4]

Received 19 November 2002; revised 8 January 2003; accepted 14 January 2003; published 5 April 2003.

[1] Recent satellite observations indicate a significant decrease of cloud water in ship tracks, in contrast to an ensemble of in situ ship-track measurements showing no average change in cloud water relative to the surrounding clouds, and contrary to the expectation of cloud water increasing in polluted clouds. We find through large-eddy simulations of stratocumulus that the trend in the satellite data is likely an artifact of sampling only overcast clouds. The simulations instead show cloud cover increasing with droplet concentrations. The simulations also show that increases in cloud water from suppressing drizzle by increasing droplet concentrations are favored at night or at extremely low droplet concentrations. *INDEX TERMS:* 3360 Meteorology and Atmospheric Dynamics: Remote sensing.
Citation: Ackerman, A. S., O. B. Toon, D. E. Stevens, and J. A. Coakley Jr., Enhancement of cloud cover and suppression of nocturnal drizzle in stratocumulus polluted by haze, *Geophys. Res. Lett.*, *30*(7), 1381, doi:10.1029/2002GL016634, 2003.

1. Introduction

[2] The effects of aerosols on clouds constitute a major uncertainty in predictions of global climate change [*Houghton et al.*, 2001]. A subset of sufficiently large and wettable aerosols serve as cloud condensation nuclei (CCN) that determine the number concentration of cloud droplets during cloud formation. The primary effect of increased concentrations of CCN is to redistribute cloud water over a greater number of droplets, thereby increasing total droplet cross-sectional area and hence cloud albedo. This effect was first suggested by *Twomey* [1974] as a mechanism by which pollution can exert a strong radiative cooling effect on global surface temperatures. Beyond the ''Twomey effect'' are possible secondary effects resulting from suppression of precipitation by smaller droplets, expected to amplify the negative radiative forcing by increasing cloud cover and cloud water [*Albrecht*, 1989].

[3] We focus on low-lying stratiform marine clouds because they cover vast areas of the global ocean, reflect much more sunlight than the underlying ocean surface, and do not appreciably affect outgoing thermal radiation. The response of clouds to regional-scale variations in CCN are invariably subject to co-varying meteorological conditions, muddling the cloud microphysical response with changes from dynamical forcings. To bypass such a tangling of signals, we consider the natural laboratory of ship tracks, which are linear features of enhanced albedo in clouds polluted by ship exhaust [*Coakley et al.*, 1987] where the only significant perturbation is the aerosol loading within the exhaust plume.

[4] The primary (or ''Twomey'') effect is robustly observed in ship tracks [*Ackerman et al.*, 2000]. Evidence for secondary effects is ambiguous. Cloud cover is seen to increase in satellite imagery of optically thin [*Conover*, 1966] and patchy clouds [*Scorer*, 1987], but some of that increase is explained by the Twomey effect. The average change of cloud water obtained from 64 in situ measurements of ship tracks during the Monterey Area Ship Tracks (MAST) project is not statistically different from zero, as shown in Figure 1 (see Appendix A). In contrast, high resolution (50-m) airborne imagery of three ship tracks during MAST indicates that cloud liquid water path (LWP) decreased on average [*Platnick et al.*, 2000], which is the opposite response expected from drizzle suppression. A more recent analysis of hundreds of 30-km segments of ship tracks from 1-km resolution satellite measurements [*Coakley and Walsh*, 2002] shows a statistically significant average decrease of LWP in ship tracks relative to the surrounding clouds (Figure 1). Here we use large-eddy simulations to investigate this apparent discrepancy between the satellite and in situ measurements.

2. Results

[5] Convection in the stratocumulus-topped marine boundary layer is driven largely by infrared cooling near cloud top [*Lilly*, 1968]. Solar heating offsets some of that cooling and thereby inhibits convection, reducing the supply of surface moisture [*Nicholls*, 1984]. In our simulations (described in Appendix B) the peak solar heating rate is $\sim$1 K h^{-1} at noon, which is 20% of the peak infrared cooling rate. As seen in Figure 2, the more vigorous nocturnal convection enhances LWP relative to the daytime, and results in greater cloud cover at night. Such diurnal tendencies were also observed in the field project from which our simulations are derived [*Cielielski et al.*, 2001]. The enhanced nocturnal LWP increases surface precipitation relative to the daytime. The daytime response of drizzle to increased droplet concentrations (N) is slight: at $N > 50$ cm^{-3} the daytime drizzle flux is already so small that reducing it further has little effect on average LWP.

[6] The most dramatic changes in LWP with N occur at the lowest droplet concentrations. At the lowest droplet concentrations there is too much drizzle to maintain a radiatively-driven, stratocumulus-topped boundary layer [*Ackerman et al.*, 1993], which is replaced by a field of shallow cumulus [*Stevens et al.*, 1998]. The transition from stratocumulus to shallow cumulus is evident in synthetic images of cloud albedo (Figure 3). The fractional area of

[1]NASA Ames Research Center, Moffett Field, California, USA.
[2]University of Colorado, Boulder, Colorado, USA.
[3]Lawrence Livermore National Laboratory, Livermore, California, USA.
[4]Oregon State University, Corvallis, Oregon, USA.

0094-8276/03/2002GL016634$05.00

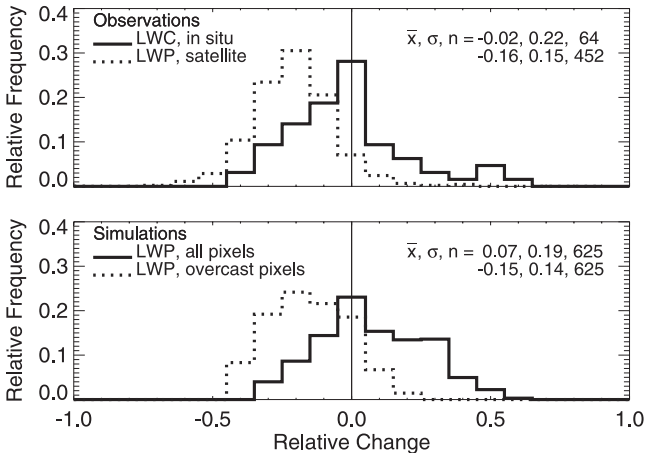

Figure 1. Frequency histograms of changes relative to the background clouds in liquid water content (LWC) measured in situ and liquid water path (LWP) from satellite measurements of ship tracks (top panel) and between model simulations with CCN number concentrations fixed at 75 and 150 cm^{-3} (bottom panel). For comparison with the satellite measurements, obtained around 4 PM local time from 30-km segments of 1-km pixels, the model output is sampled every 5 minutes from 3–5 PM, and differences taken between domain averages. A pixel is considered overcast in the simulations if the optical depth in 90% of its 256 model columns exceeds 2.5. Mean value, standard deviation, and total number of samples are listed for each distribution.

convective cloud cores is ~1/2 in the stratocumulus, but falls below that level at the lowest droplet concentrations (Figure 2c). The fractional cloud cover approaches that of convective cores at the lowest droplet concentrations, indicating that cloudy air detrained from convective cores does not extend far from those cores.

[7] The cumuliform convection of the clean boundary layer results from increased atmospheric stability, in which weaker eddies are resisted and vertical mixing is dominated by the strongest eddies. The increased atmospheric stability at reduced N results from more cooling below cloud base by greater drizzle evaporation [*Nicholls*, 1984] and greater drying near cloud top by drizzle formation. The drying diminishes the infrared cooling [*Ackerman et al.*, 1993], and decreases the (convectively favorable) latent cooling of cloudy air during descent [*Stevens et al.*, 1998]. However, this cumuliform convection is highly susceptible to changes in aerosol populations, as found in field measurements [*Taylor and Ackerman*, 1999] and model simulations [*Stevens et al.*, 1998].

[8] During extremely clean conditions, the injection of ship exhaust has been observed to rapidly transform shallow, cumuliform clouds in the boundary layer into a prominent cloud line [*Taylor and Ackerman*, 1999]. Visible ship tracks are seen most often in cloud fields that are patchy [*Scorer*, 1987]. Such tracks, however, are not included in satellite observations restricted to overcast conditions. Our daytime simulations at a droplet concentration of ~50 cm^{-3} (CCN concentration = 75 cm^{-3}) are more microphysically representative of the satellite background conditions, with comparable cloud droplet effective radii (r_{eff}) of 13.5 μm for the satellite data and 14.0 μm for the simulated clouds. As the droplet concentration doubles and average r_{eff} decreases by 3.1 μm, the domain-average daytime LWP changes little in the simulations (Figure 2a), in contrast with the 15% average reduction of LWP in ship tracks indicated by the satellite data (Figure 1). However, the satellite observations were restricted to overcast pixels, and our simulations indicate that cloud cover continues to increase with $N > 50$ cm^{-3} (Figures 2c and 3).

[9] Omitting cloud-free and partly cloudy pixels artificially enhances LWP, and the magnitude of this enhancement increases with the number of pixels omitted. As shown in Figures 2a and 4, there is little change in the daytime domain-average LWP between CCN concentrations of 75 and 150 cm^{-3}. But as the concentration of CCN increases, the distribution of LWP narrows. The smaller concentration of CCN results in a distribution of LWP that is broader and skewed toward smaller values. Once a threshold is applied, as commonly done in imagery analysis to identify overcast fields of view, the distribution of LWP at the lower CCN concentration yields a greater number of cloud-free and partly cloudy pixels that fall below the overcast threshold. As a result, the difference between the domain-average LWP and the average LWP for the overcast pixels is greater at the lower CCN concentration. The upper panels of Figure 4 show that the difference between the domain-average LWP and the average for the overcast pixels is 40% at a CCN concentration of 75 cm^{-3} but only 10% at a CCN concentration of 150 cm^{-3}. Since the domain-average LWP only increases 5% as the CCN concentration doubles, the average LWP in overcast pixels is smaller at the greater CCN concentration.

[10] The changes in LWP depend not only on the changes in CCN populations (and surely meteorology) but also on the definition of overcast. *Coakley and Walsh* [2002] use

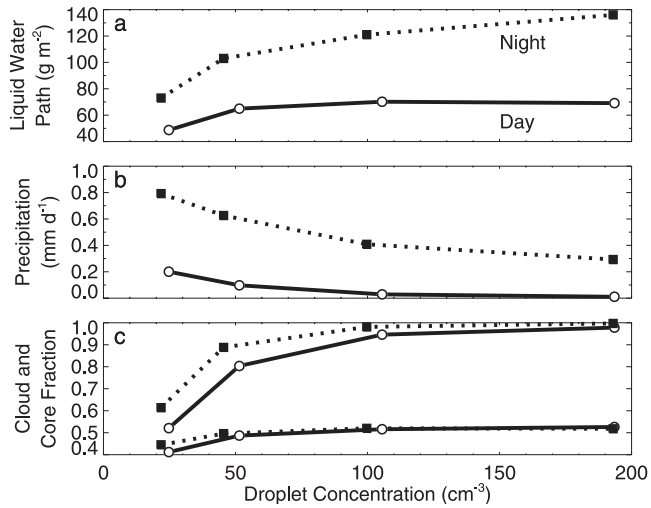

Figure 2. Domain-average properties from daytime (circles) and nocturnal (squares) simulations with CCN number concentrations of 40, 75, 150, and 300 cm^{-3}. Plotted against the cloud droplet concentration, averaged over grid cells with LWC > 0.05 g cm^{-3}, are (a) LWP, (b) surface precipitation rate, and (c) fractional cloud cover (upper curves, defined as in [*Wyant et al.*, 1997] by the fraction of model columns with optical depth > 2.5) and maximum core fraction (lower curves, where core fraction is defined as in *Stevens et al.* [2001] by the fractional number of cloudy, buoyant grid cells in each model layer). The data are averaged over the last 10 h of 12 h simulations.

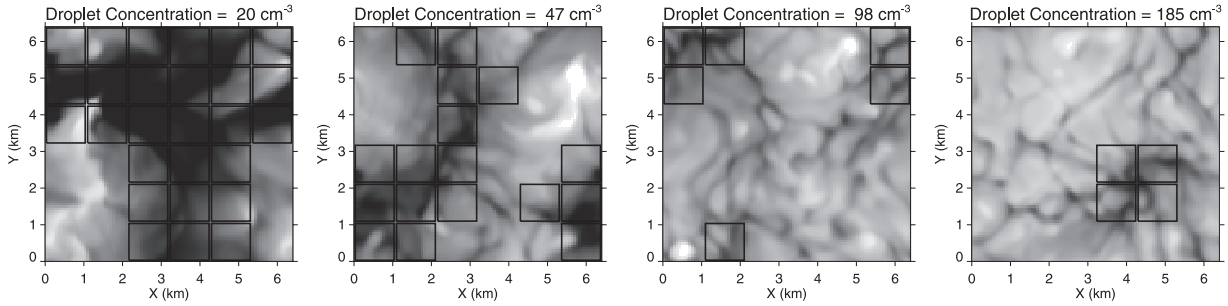

Figure 3. Cloud albedo at 3 PM local time in simulations with CCN concentrations fixed at 40, 75, 150, and 300 cm^{-3} from left to right. The average cloud droplet concentration in cloudy grid cells (as in Figure 2) for each scene is given. Dark squares outline 1.1 × 1.1 km regions that are < 90% cloudy (defined in Figure 1).

variability within 4 × 4 km regions to select only overcast pixels. We instead apply an optical depth threshold at a much smaller horizontal scale (∼65 m), yet the change at the low end of the LWP distribution between the background clouds and ship tracks compares favorably with that for the overcast pixels in the simulations (lower panels of Figure 4). The application of an optical depth threshold shifts the LWP distribution to smaller values as the CCN concentration increases. If we relax our optical depth threshold for cloudy columns from 2.5 to 1, the relative reduction of LWP within the overcast pixels is reduced by 1/2.

[11] As a result of the transition from cumuliform to stratiform convection, at droplet concentrations below ∼50 cm^{-3} the fractional area of convective cloud cores increases with N (Figure 2c). As N increases further, the decreasing drizzle flux does not change domain-average daytime LWP appreciably in our simulations, but rather redistributes it spatially. Detrained cloudy air is less desiccated by the reduced drizzle within the cloud, and hence evaporates more slowly in the clear areas between convective cores, which is the essence of *Albrecht*'s [1989] argument for cloud cover increasing with the lifetime of cloudy air. Visible cloud boundaries also encroach on the clear air through the enhanced total droplet cross-sectional area at greater N, which is effectively the Twomey effect applied to detraining cloudy air.

[12] The narrowing of the frequency distribution of LWP for polluted clouds in our simulations can resolve the apparent discrepancy between the decrease in LWP for polluted clouds as inferred from satellite imagery and the constant LWC as inferred from in situ observations. The narrowing arises because the liquid water distribution becomes more spatially uniform. Because of the narrowing LWP distribution, clouds at reduced CCN concentrations will show a greater difference between domain-average LWP and the average LWP for overcast pixels. In contrast, the in situ aircraft observations of LWC are averaged over comparable flight lengths, whether cloudy or clear, thus avoiding any apparent shifts in the LWC that might arise by limiting the averages to cloudy air. These different measurement strategies could well explain the different outcomes of the satellite and in situ studies. However, the inherent difference between LWP, as deduced from satellites, and LWC, from in situ observations, also complicates comparisons between the observations.

3. Conclusions

[13] We have shown that the in situ measurements and satellite retrievals of ship track cloud water can be reconciled if cloud cover increases with droplet concentrations, as in our simulations. Relying only on cloud properties from overcast pixels to infer the effects of aerosols on clouds is a commonly used strategy that we find can be misleading. We recommend that future studies of remotely-sensed cloud measurements assess the impact of the overcast approximation on the effects of aerosols on clouds and explicitly address the fraction of pixels not counted as overcast. We also recommend that high-resolution remote sensing [e.g., *Platnick et al.*, 2000] be brought to bear on the issues we have raised.

[14] Our analysis suggests that increases in cloud water with increasing droplet concentrations are favored at night or under extremely low droplet concentrations. By modulating the aerosol-induced suppression of drizzle, sunlight substantially limits the increase in solar reflectivity of marine stratocumulus polluted by haze and provides a physical limitation on the indirect radiative forcing of aerosols.

[15] Beyond the behavior at extremely low ambient CCN concentrations, in which ship tracks appear as prominent cloud lines in visible satellite imagery, we expect the cloud-free gaps within ship-track clouds to fill in, resulting in

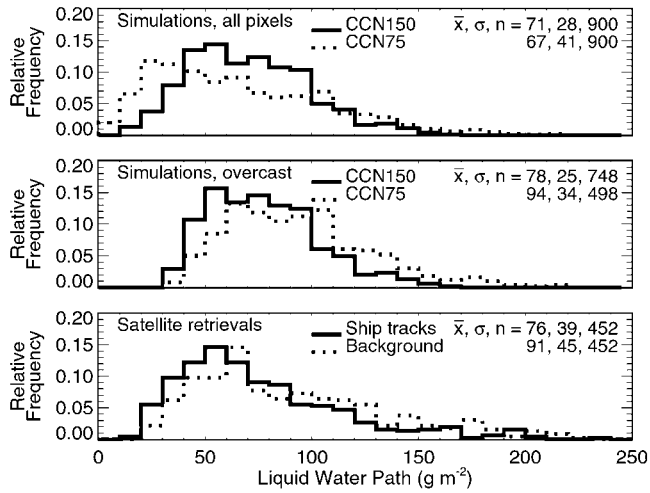

Figure 4. Frequency histograms of LWP for all (top panel) and overcast (middle panel, as defined in Figure 1) 1–km pixels from 3–5 PM with CCN concentrations fixed at 150 and 75 cm^{-3} for the solid and dotted lines, respectively. Bottom panel shows distributions of LWP for satellite observations of ship tracks (solid lines) and background clouds (dotted lines) averaged over 30-km segments. Other notation as in Figure 1.

observable increases in fractional cloud cover compared to the surrounding regions. We also expect the liquid water path in ship tracks to be enhanced relative to surrounding clouds in the morning because of greater drizzle suppression at night.

Appendix A: Filtering of in situ Measurements

[16] We omit from the ensemble of *Ackerman et al.* [2000] the five penetrations of the Sanko Peace ship track, in which the marine boundary layer was observed to rapidly deepen on a day in which extremely low droplet concentrations were measured in the background clouds [*Taylor and Ackerman*, 1999]. A composited profile of LWC shows LWP increasing significantly in the ship track. Because we bin relative changes in LWC with respect to the background cloud, we must omit the data above the background cloud tops where that relative change is infinite. This leaves us to consider the data from flight levels within the background clouds. At those altitudes, drying caused by entrainment of air from above the boundary layer reduced LWC in the ship track. Including only the decrease of LWC measured in those five penetrations would misrepresent the positive LWP change. Hence we omit those five penetrations because they are biased negatively with respect to LWP in the satellite data.

Appendix B: Description of Model Simulations

[17] The dynamical core of the numerical model is described by *Stevens et al.* [2002] and the cloud microphysics and radiative transfer are described by *McFarlane et al.* [2002]. Here we use a domain spanning 6.4×6.4 km horizontally and 1.5 km vertically, which is discretized into $96 \times 96 \times 50$ equal volume grid cells. A sponge layer at the top of the model dampens trapped buoyancy waves at altitudes >1250 m. Subsidence and radiative forcings are linearly attenuated to zero in the 300 m above the inversion (defined as the average height where the total water mixing ratio exceeds 8.5 g kg^{-1}) to prevent drift of the overlying atmospheric properties resulting from any imbalanced forcings [*Stevens et al.*, 2001]. The particle size distributions are resolved into 20 bins over a range from 0.01 to 4.3 μm radius for ammonium bisulfate CCN, and over a range from 1 to 430 μm radius for activated cloud droplets. The total particle number concentration is fixed in each simulation and thus the distribution of unactivated CCN in each grid cell is computed from the droplet distribution and the initial CCN distribution. The initial CCN distribution is log-normal with a geometric mean radius of 0.1 μm and a geometric standard deviation of 1.2.

[18] Our simulations are based on an idealization of the First Lagrangian case study from the Atlantic Stratocumulus Transition Experiment [*Duynkerke et al.*, 1995], with model initialization and forcings adapted from the Fourth International Cloud Modeling Workshop (12–16 August 1996, Clermont-Ferrand, France, sponsored by the Global Energy and Water Experiment (GEWEX) Cloud System Studies (GCSS)). We depart from those specifications by initializing our model domain as initially cloud free, with the initial relative humidity limited to < 99%, and using surface similarity for surface fluxes, with the sea surface temperature fixed at 290.4 K. Additionally, in place of a parameterized infrared cooling of up to 74 W m^{-2} in the workshop specification, we use a two-stream radiative transfer model in which the water vapor column overlying the model domain is fixed at 1.5 g cm^{-2}, resulting in a net upward infrared flux of 80 W m^{-2} above the boundary layer after the cloud layer forms. Solar radiation is calculated for summer solstice at 38° latitude, with time zero corresponding to 6 AM locally. Radiative transfer is calculated for each column every 2 minutes.

[19] By simply changing CCN concentrations over the entire model domain between simulations, we do not simulate the lateral dispersion of ship tracks, but rather the contrasts between ship tracks and surrounding clouds on scales smaller than the width of mature ship tracks (often > 10 km), representative of regional scale variations in aerosol plumes from larger sources.

[20] **Acknowledgments.** We thank Steve Platnick for helpful comments. This work was supported by the NASA Global Aerosol Climatology Project.

References

Ackerman, A. S., et al., Dissipation of marine stratiform clouds and collapse of the marine boundary layer due to the depletion of cloud condensation nuclei by clouds, *Science*, *262*, 226–229, 1993.

Ackerman, A. S., et al., Effects of aerosols on cloud albedo: Evaluation of Twomey's parameterization of cloud susceptibility using measurements of ship tracks, *J. Atmos. Sci.*, *57*, 2684–2695, 2000.

Albrecht, B., Aerosols, cloud microphysics, and fractional cloudiness, *Science*, *245*, 1227–1230, 1989.

Cielielski, P. E., et al., Diurnal variability of the marine boundary layer during ASTEX, *J. Atmos. Sci.*, *58*, 2355–2376, 2001.

Coakley, J. A., Jr., and C. D. Walsh, Limits to the aerosol indirect radiative effect derived from observations of ship tracks, *J. Atmos. Sci.*, *59*, 668–680, 2002.

Coakley, J. A., Jr., et al., Effect of ship-stack effluents on cloud reflectivity, *Science*, *237*, 1020–1022, 1987.

Conover, J. H., Anomalous cloud lines, *J. Atmos. Sci.*, *23*, 778–785, 1966.

Duynkerke, P. G., et al., Microphysical and turbulent structure of nocturnal stratocumulus as observed during ASTEX, *J. Atmos. Sci.*, *52*, 2763–2777, 1995.

Houghton, J. T., et al. (Eds.), *Climatic Change 2001: The Scientfic Basis*, Cambridge Univ. Press, New York, 2001.

Lilly, D. K., Models of cloud-topped layers under a strong inversion, *Q. J. R. Meteorol. Soc.*, *94*, 292–309, 1968.

McFarlane, S., et al., A Bayesian algorithm for the retrieval of liquid water cloud properties from microwave radiometer and millimeter radar data, *J. Geophys. Res.*, *107*(D16), 4317, doi:10.1029/2001JD001011, 2002.

Nicholls, S., The dynamics of stratocumulus: Aircraft observations and comparisons with a mixed layer model, *Q. J. R. Meteorol. Soc.*, *110*, 783–820, 1984.

Platnick, S., et al., The role of background cloud microphysics in the radiative formation of ship tracks, *J. Atmos. Sci.*, *57*, 2607–2624, 2000.

Scorer, R. S., Ship trails, *Atmos. Environ*, *21*, 1417–1425, 1987.

Stevens, B., et al., Large-eddy simulations of strongly precipitating, shallow, stratocumulus-topped boundary layers, *J. Atmos. Sci.*, *55*, 3616–3638, 1998.

Stevens, B., et al., Trade-wind cumuli under a strong inversion, *J. Atmos. Sci.*, *58*, 1870–1891, 2001.

Stevens, D. E., et al., Effect of domain size and numerical resolution on the simulation of shallow cumulus convection, *J. Atmos. Sci.*, *59*, 3285–3301, 2002.

Taylor, J. P., and A. S. Ackerman, A case-study of pronounced perturbations to cloud properties and boundary-layer dynamics due to aerosol emissions, *Q. J. R. Meteorol. Soc.*, *125*, 2643–2661, 1999.

Twomey, S., Pollution and the planetary albedo, *Atmos. Environ.*, *8*, 1251–1256, 1974.

Wyant, M. C., et al., Numerical simulations and a conceptual model of the stratocumulus to trade cumulus transition, *J. Atmos. Sci.*, *54*, 168–192, 1997.

A. S. Ackerman, NASA Ames Research Center, Moffett Field, CA 94035, USA. (ack@sky.arc.nasa.gov)

J. A. Coakley Jr., Oregon State University, Corvallis, OR 97331, USA. (coakley@coas.oregonstate.edu)

D. E. Stevens, Lawrence Livermore National Laboratory, Livermore, CA 94552, USA. (dstevens@llnl.gov)

O. B. Toon, University of Colorado, Boulder, CO 80309, USA. (btoon@lasp.colorado.edu)